Reductions in atmospheric levels of non-CO2 greenhouse gases explain about a quarter of the 1998-2012 warming slowdown

Xuanming Su, Hideo Shiogama, Katsumasa Tanaka, Kaoru Tachiiri, Tomohiro Hajima, Michio Watanabe, Michio Kawamiya, Kiyoshi Takahashi, Tokuta Yokohata

communications earth & environment

Article

https://doi.org/10.1038/s43247-024-01723-x

Reductions in atmospheric levels of non-CO_2 greenhouse gases explain about a quarter of the 1998-2012 warming slowdown

Xuanming Su [1,2] ✉, Hideo Shiogama [3], Katsumasa Tanaka [3,4], Kaoru Tachiiri[1], Tomohiro Hajima [1], Michio Watanabe [1], Michio Kawamiya [1], Kiyoshi Takahashi [2] & Tokuta Yokohata [3]

The observed global mean surface temperature increase from 1998 to 2012 was slower than that since 1951. The relative contributions of all relevant factors including climate forcers, however, have not been comprehensively analyzed. Using a reduced-complexity climate model and an observationally constrained statistical model, here we find that La Niña cooling and a descending solar cycle contributed approximately 50% and 26% of the total warming slowdown during 1998-2012 compared to 1951-2012. Furthermore, reduced ozone-depleting substances and methane accounted for roughly a quarter of the total warming slowdown, which can be explained by changes in atmospheric concentrations. We identify that non-CO_2 greenhouse gases played an important role in slowing global warming during 1998-2012.

Observations implied a slower global temperature increase over 1998–2012 relative to 1850–1900 (ΔT) in comparison to the warming from 1951–2012, despite the rapid growth in greenhouse gas (GHG) emissions during the same period[1]. The difference of decadal trends (DDT), that is, the decadal trend of 1998–2012 minus that of 1951–2012, indicated a negative value. Newer temperature records with updated sea surface temperature (SST) datasets and the infilling of missing data in places such as the Arctic showed greater positive trends, implying that the slowing was not as severe as previously thought[2]. For example, the latest Met Office Hadley Centre/Climatic Research Unit global surface temperature anomalies, version 5 (HadCRUT5), used by default in this study, showed an apparently less negative DDT (-0.011 °C per decade) compared to the older version of HadCRUT4.6 (-0.055 °C per decade) (Supplementary Fig. 1). Such a slowing trend may differ among independent observations. Nonetheless, there is no doubt that a warming slowdown does exist[3]. The Sixth Assessment Report (AR6) of the Intergovernmental Panel on Climate Change (IPCC) referred to this phenomenon as a temporary event[4], primarily due to internal variability[5–10] and natural forcings such as volcanic and solar irradiance[3,11–16]. The strengths of internal variability or natural forcings, however, are uncertain[1,4,17,18]. Reductions in methane and ozone-depleting substances (ODS)[19,20] or stratospheric water vapour[21] may also have contributed, but their respective impacts have not been explicitly calculated. Furthermore, warming slowdown cannot be described by a single factor; rather, it necessitates an integrated influence combining multiple components, such as internal variability, forcing changes, ocean heat uptake, and insufficient observational coverage[15,22–25]. Quantifications of relative contributions from these individual components are important to interpret the causes of the warming slowdown.

Physical climate models may insufficiently capture the internal variability or underestimate the response to solar irradiance change[3], resulting in a higher-than-observed ΔT during the warming slowdown period[4]. Statistical models, on the other hand, can capture ΔT variations but strongly depend on the chosen predictors and their time lags and usually use the whole anthropogenic influence as an input[3,11,26], hindering further attributions at the emission level. A systematic and reliable assessment of the individual contributing factors to the warming slowdown has not been conducted to our knowledge. Here, we combined a reduced-complexity model (RCM) used to quantify the ΔT trends caused by individual climate forcers with a statistical regression model to reconcile the causes with the observed ΔT.

[1]Research Institute for Global Change/Research Center for Environmental Modelling and Application, Japan Agency for Marine-Earth Science and Technology (JAMSTEC), Yokohama, Japan. [2]Social Systems Division, National Institute for Environmental Studies(NIES), Tsukuba, Japan. [3]Earth System Division, National Institute for Environmental Studies (NIES), Tsukuba, Japan. [4]Laboratoire des Sciences du Climat et de l'Environnement (LSCE), IPSL, CEA/CNRS/UVSQ, Université Paris-Saclay, Gif-sur-Yvette, France. ✉e-mail: suxuanming@jamstec.go.jp

Attribution of anthropogenic and natural ΔT

First, we applied a normalized marginal approach[27–29] to an RCM, the Simple Climate Model for Optimization version 3.3 (SCM4OPT v3.3)[30–33], to quantify the ΔT trends for respective climate forcers (Methods). Second, we used a regression statistical model[3,11,26] to decode the impacts of anthropogenic and natural factors. This was a twofold approach: the regression can correct the biases in the magnitude of the simulated ΔT, while the relative contributions of external forcing factors and internal variability to the observed ΔT are decomposed. To avoid overfitting, we tested a group of statistical models with different predictors and chose the one with the lowest Bayesian information criterion (BIC) (Supplementary Table 1). The monthly observed ΔT was then modelled as a multiple regression of anthropogenic factors, natural forcings, El Niño and Southern Oscillation (ENSO), and residuals, allowing for errors in simulations and observations (Methods). As a result, we decomposed the observed ΔT into ΔT caused by each anthropogenic factor, such as CO_2, CH_4, N_2O, ODS, other fluorinated gases, aerosols and pollutants, and land use albedo, as well as each natural factor, such as volcanic eruptions, solar irradiance, and ENSO (Fig. 1). The

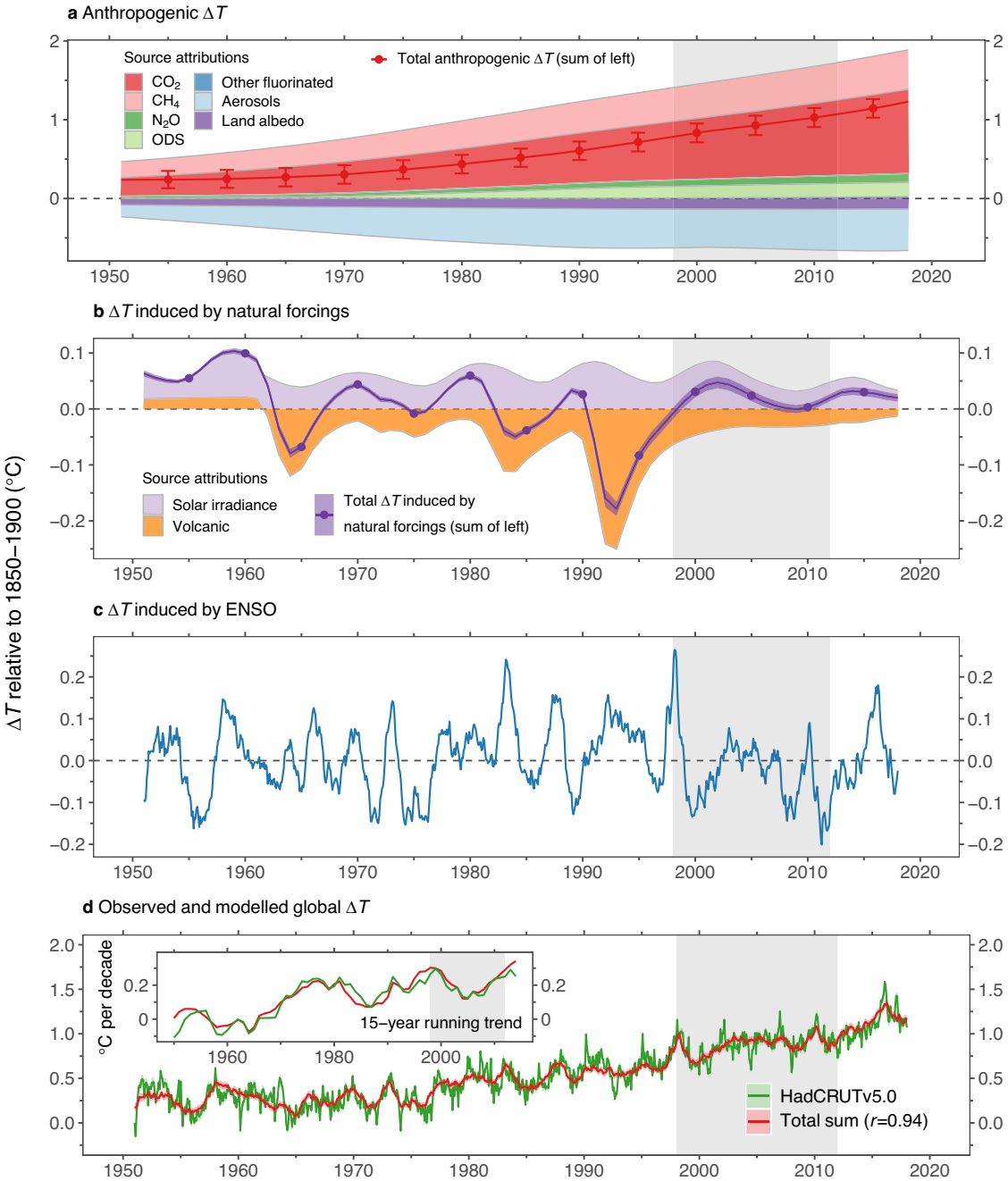

Fig. 1 | Anthropogenic and natural ΔT. **a** Anthropogenic ΔT. The thick red solid line and error bars indicate total anthropogenic ΔT. **b** ΔT caused by natural forcings. The thick purple solid line and range represent the total ΔT induced by natural forcings. Colour ribbons in **a** & **b** show ΔT caused by individual factors. **c** ΔT caused by ENSO. **d** HadCRUT5 and the total summed ΔT. Pearson's correlation between the total sum and HadCRUT5 is shown in **d**. The inset in **d** depicts 15-year running trends. The error bar in **a** and ranges in **b**–**d** are the one-sigma produced by the ensemble of statistical regressions. Note that the range of uncertainty may be very narrow and not represented in the figure; see Data availability for the details. See Methods for further information on estimating uncertainty. The warming slowdown era from 1998 to 2012 is shaded in light grey.

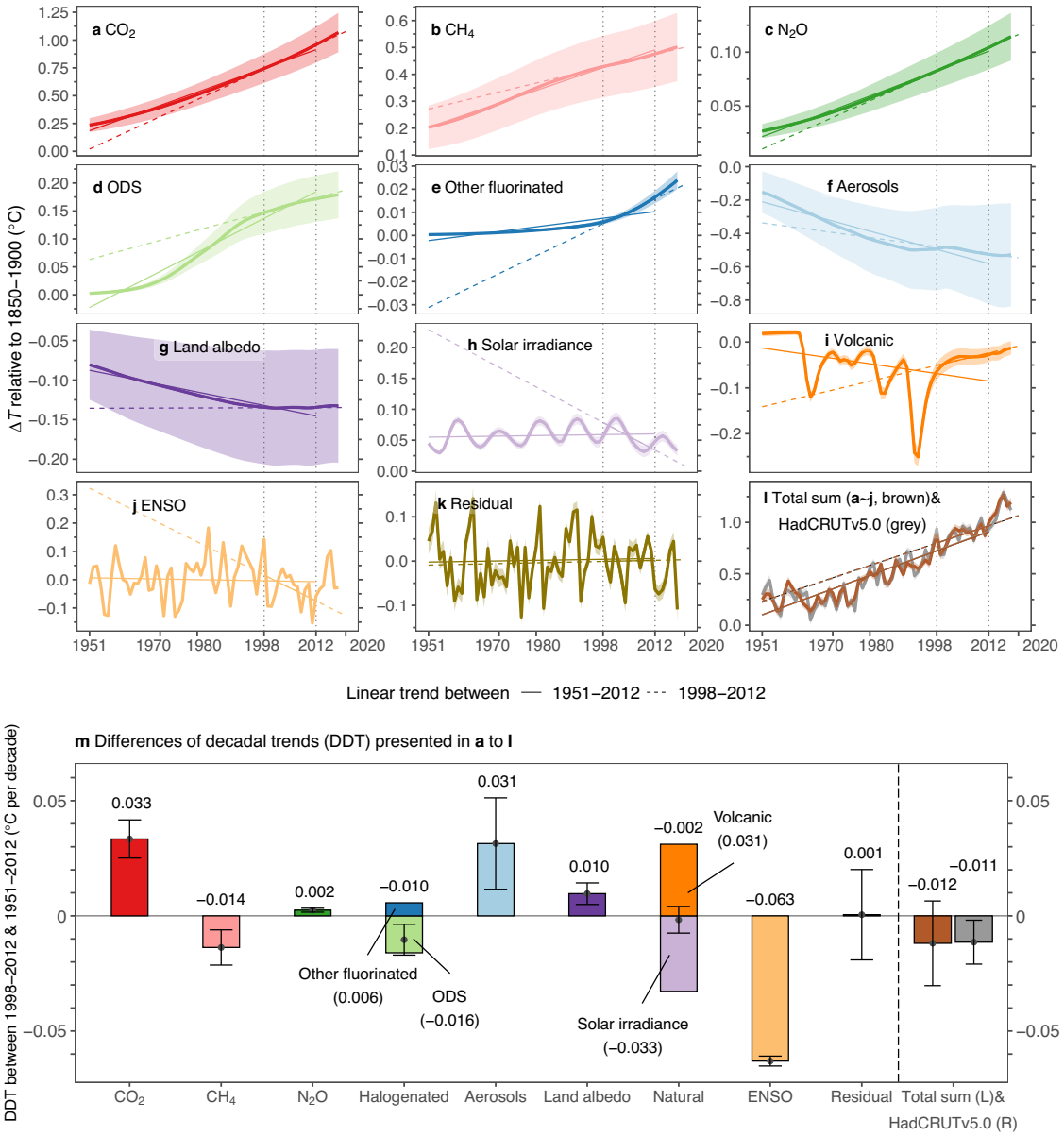

Fig. 2 | Anthropogenic and natural ΔT by source and their DDT between 1998–2012 and 1951–2012. a to **j** represent ΔT and uncertainty ranges caused by individual anthropogenic and natural factors. **k** indicates the residual term of the statistical model. The total sum and HadCRUT5 and their uncertainty ranges are depicted in **l**. Thin solid and solid with extended dashed lines denote linear trends from 1951 to 2012 and 1998 to 2012, respectively. **m** illustrates DDT derived from **a** to **l**. The mean is displayed on top of the bar, and the error bar is the one-sigma produced by the ensemble of statistical regressions.

modelled ΔT and the observed ΔT showed a strong positive correlation (r = 0.94, 1951-2018). The 15-year running trends of both variables were consistent, as shown in the inset of Fig. 1d. This suggests that our study successfully captured most of the changes in the observed ΔT.

Results

Methane stabilization and ODS mitigation help slow global warming

Figure 2a–l shows ΔT attributions by source, residuals, the total sum of all sources, and the observed ΔT HadCRUT5 to aid comparison. Gradients indicated by the thin solid and solid with extended dashed lines represent ΔT linear trends from 1951 to 2012 and from 1998 to 2012, respectively. Accordingly, to the left of the junction, if the dashed line is above the solid line, it implies that the growth rate is slowing, and vice versa. Methane, ODS, solar irradiance, and ENSO negatively contributed to ΔT during 1998-2012 compared to 1951-2012. The emission attributions of ΔT agree mostly with the AR6 forcing-based estimate[34] (Supplementary Fig. 2), except for halogenated ΔT, which is approximately twice as high as AR6. This is because our method generated a small negative ODS-induced stratospheric ozone radiative forcing (denoted as ΔF, referring to forcing increases above the preindustrial level) (-0.05 ± 0.03 Wm^{-2}, 1850-2012), consistent with previous studies (ranging from -0.03 to -0.1 Wm^{-2} [35–39]). Consequently, a minor ΔF was canceled from the GHG impact of ODS (0.31 ± 0.01 Wm^{-2}, 1850-2012), and the net ODS ΔF was positively larger in our results. Other studies revealed a far higher cancellation rate, up to 80%[40,41]. In this instance, the resulting net ODS effect will be smaller than in our study.

Based on the attributed ΔT, we computed the decadal trend (Supplementary Fig. 3) and DDT (Fig. 2m) for each source. Note that DDT was also affected by the referred historical period; selecting a shorter period of 1970-2012 would highlight such a slowdown more clearly because ΔT increased more rapidly throughout 1970-2012 (Supplementary Fig. 1). However, we examined 1951-2012 for a general case as suggested in the IPCC reports[1,4].

ENSO contributed the most to the warming slowdown, with a DDT of -0.063 ± 0.002 °C per decade, followed by solar irradiance (-0.033 ± 0.002 °C per decade). Anthropogenic ODS (-0.016 ± 0.007 °C per decade) and methane (-0.014 ± 0.008 °C per decade) also contributed to the warming slowdown. Specifically, ENSO and solar variations diminished warming directly with a negative decadal trend, while ODS and methane emissions simply exhibited a smaller decadal trend during 1998-2012 compared to that of 1951-2012. Other sources, including CO_2, N_2O, other fluorinated gases, aerosols and pollutants, land albedo, and volcanic activity, showed positive DDT, meaning that they increased faster between 1998 and 2012 than they did between 1951 and 2012. It is worth noting that the ΔT of total GHG emissions increased steadily (DDT 0.012 ± 0.015 °C per decade, Supplementary Fig. 4), masking the slowdown of ODS and methane ΔT (Supplementary Fig. 5), which is likely why previous research missed them. In addition, aerosols and pollutants and land albedo (see Supplementary Fig. 6 for the forcing trends) contributed to negative warming over 1951–2012. However, during the warming slowdown period, their downward tendencies slowed and contributed to a positive DDT (see Supplementary Fig. 7).

The slowdown of methane ΔT can be explained by the associated atmospheric concentrations (denoted as ΔC). Growth in methane ΔC is reported to have slowed from the 1980s and to have stabilized between 1999 and 2006[42–47], owing to the notable methane reductions in the agriculture sector in Europe and Russia, as well as in the energy sector in Europe, Japan, the Middle East and Russia, before or during the warming slowdown period. These reductions may, in part, offset the rapid growth in methane emissions in China and India (Supplementary Fig. 8)[48,49]. As shown in Fig. 3a, the DDT of methane ΔC simulated by SCM4OPT v3.3 presented a negative value of -52.4 ppb per decade, indicating that methane ΔC slowed prominently during the warming slowdown period, which partly explains the slowdown of methane ΔT at the same time.

ODS manifested consistent DDT between the simulated ΔC (-224.9 CFC-12 equivalent ppt per decade) and the observed ΔC (CMIP6 -212.5 CFC-12 equivalent ppt per decade) (Fig. 3b) because they are well documented[46,47,50]; hence, ΔC can be well captured by the model. ODS have been effectively mitigated under the Montreal Protocol since the late 1980s, particularly for CFC-11, CFC-12 and CFC-113 (Supplementary Fig. 9)[51], resulting in a stabilized mixing ratio in the atmosphere. Such a tendency can also be used to interpret the negative DDT of ODS ΔT. The ΔC of other GHGs, including CO_2, N_2O and other fluorinated gases, however, continued to rise, accelerating ΔT rather than slowing it during the warming slowdown era (Supplementary Fig. 10).

Contributions of natural forcing factors and ENSO

As shown in Fig. 4a, our natural forcing ΔT is in line with results from previous RCMs[52] as well as more complex Earth system models (ESMs)[53] (for GHGs and aerosols and pollutants, see Supplementary Figs. 5&11). Figure 4b depicts volcanic ΔF and ΔT. Although volcanic ΔF had a negative DDT (-0.045 Wm^{-2} per decade), recovery from the cooling caused by large volcanic activities in the 20th century caused a long-term negative trend (-0.012 °C per decade, 1951–2012), whereas weak volcanic activity in the 1998–2012 period caused a small positive trend (0.019 °C per decade, 1998–2012), resulting in a positive DDT. In the case of solar irradiance (Fig. 4c), the decadal trends for both ΔF and ΔT became slower during 1998–2012 compared to 1951–2012. Thus, we can pin at least some of the cooling on the descending solar cycle. Regarding volcanic aerosols, in contrast to earlier studies[12,14,15], which could balance out up to 30% of anthropogenic ΔT[3], our results suggest that volcanic forcing is not responsible for the warming slowdown. Our result also implies a relatively large contribution from the descending solar cycle, similar to Lean (2018)[3], which mitigated approximately 36% of anthropogenic ΔT from 2001 to 2011. However, Lean (2018) also showed a small 8% cut in anthropogenic ΔT from volcanic aerosols at the same time, possibly due to the use of stratospheric aerosol optical depth (AOD) to estimate volcanic ΔT in her study, which is a proxy of volcanic aerosol ΔF. The volcanic ΔF actually presented a relatively small negative decadal trend (-0.046 Wm^{-2} per decade, blue thin dashed line in Fig. 4b) from 1998-2012, which could produce the small volcanic cooling effect reported by Lean (2018). From 1998 to 2012, the decadal trend of volcanic ΔF was negative, but the decadal trend of volcanic ΔT was estimated to be positive, possibly due to the ocean's thermal inertia[16,54,55].

ENSO was a major contributor to the warming slowdown, which was mainly led by strong La Niña cooling immediately after El Niño warming prior to 1998[4,5] (Fig. 4d). Because of its seasonality, ENSO contributed to the warming slowdown in the form of an annual pulse signal (Supplementary Figs. 12–15), whereas the descending solar cycle, ODS, and methane had a relatively continuous and stable influence on warming slowdown. Our result is consistent with that of Lean (2018), which signifies the largest contribution from ENSO, with a cooling decadal trend of -0.086 °C per decade from 2001-2011 (cf. -0.065 °C per decade from 1998-2012 in this study, see Supplementary Fig. 3). It should be pointed out that anthropogenic forcing could affect La Niña like SST trends, potentially influencing ENSO[56–58]. Nevertheless, even with the utilization of more intricate ESMs, it remains challenging to identify the inherent connection. This presents a potential avenue for further research on this subject.

Warming slowdown and other abnormal climate changes

Our approach is able to explain abnormal climate changes. We identified five distinct troughs along the 15-year running trend in observed ΔT (Fig. 5). The 2005 trough, which occurred in the middle of the warming slowdown, can be intuitively explained by factors with a clear downward trend, such as methane, ODS, solar irradiance and ENSO. A weaker trough in 1994 was likely driven by a combination of methane, ODS and ENSO, whereas a remarkable 1987 trough was mostly produced by volcanic eruptions. In addition, aerosols and pollutants, solar irradiance, volcanic activity, and ENSO may have contributed to the observed ΔT troughs that occurred in 1959 and 1964, when it was deemed a global cooling phase[59].

Discussion and conclusions

An important caveat is that we estimated a less negative DDT of methane ΔC in this study (Fig. 3a), while the actual methane ΔC (for instance, DDT of CMIP6 ΔC -88.6 ppb per decade) might have contributed a more negative DDT in methane ΔT. It is because we assumed that the increase in atmospheric methane ΔC over the preindustrial level was mostly attributable to the anthropogenic sources[60–62]. However, the methane emissions from natural sources were not small[63], and these natural sources and sinks might also have contributed to the methane ΔC which was not considered here due to data availability. Furthermore, our calculations did not include the methane emissions from ultraemitters in the oil and gas industry, which contribute up to 12% of global methane emissions from oil and gas production and transmission[64]. A more accurate study of anthropogenic and natural methane emission budgets would help improve the reliability of the estimates in this study.

The emission-based attribution takes chemical-physical changes in the atmosphere into account. Methane ΔT, for example, includes ΔT produced by atmospheric methane ΔC, stratospheric water vapour from methane oxidation, the feedback on tropospheric ozone and on sinks of halogenated gases, and CO_2 from oxidized methane. Concerning ODS ΔT, their contributions contain ΔT caused by ODS ΔC and its feedback on stratospheric ozone and on methane sinks (Fig. 3b). A minor difference might exist between the ΔT resulting from ΔC and the associated emissions, but their major trends are consistent (Fig. 3, Supplementary Fig. 10). Therefore, the slowdown of ODS and methane ΔT during the warming slowdown can be robustly explained by their slowing trends in atmospheric ΔC. It is important to note that the slowing trends for both ΔC and ΔT induced by ODS and methane occurred earlier than 1998-2012, which also contributed to the warming slowdown.

Additionally, the forcing-based attribution demonstrates that natural forcing agents such as volcanic activity, solar irradiance, and ENSO tally with the emission-based attribution (Supplementary Fig. 16). However,

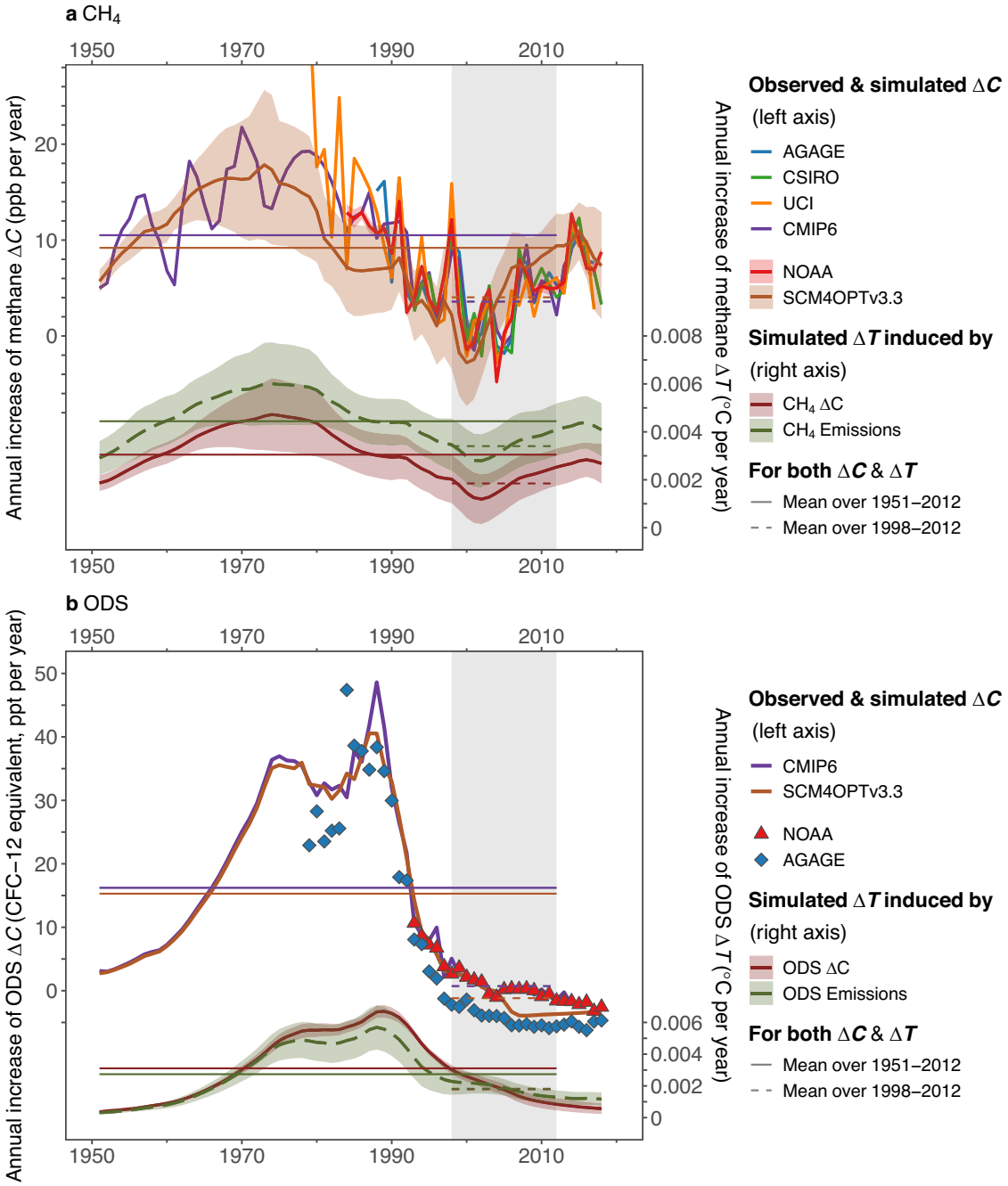

Fig. 3 | Annual increase of methane and ODS ΔC and the induced ΔT. **a** and **b** represent methane and ODS, respectively. The annual increase is defined as the value added in the current year over the previous year. The SCM4OPT v3.3 uncertainties in **a** and **b** are the one-sigma of the Monte Carlo simulation with $n = 1000$. ΔT uncertainty ranges in **a** and **b** are the one-sigma produced by the ensemble of statistical regressions. In **b**, the ODS components for each source differ (Supplementary Table 2). Uncertainty is not considered in ODS ΔC because it is an equivalent value combining a collection of compounds of ODS[47]. CMIP6[47] and SCM4OPT v3.3 contain data for the entire evaluation period. Mean values from 1951 to 2012 and 1998 to 2012 are illustrated by thin horizontal solid and dashed lines, respectively. The warming slowdown era from 1998 to 2012 is shaded in light grey.

forcing agents from anthropogenic sources are redistributed among the available components. For example, methane, ODS, tropospheric ozone, and stratospheric water vapor from methane oxidation all had a negative impact on DDT, whereas positive influences came predominantly from CO_2, N_2O, HFC, stratospheric ozone, land albedo, BC on snow, aerosols, and clouds. It should be highlighted that the forcing-based attribution for anthropogenic sources is consistent with the emission-based approach. Forcing-based CO_2 contains contributions from both CO_2 emissions and CO_2 from methane oxidation. For ODS, forcing-based attribution reflects the effects as GHGs, whereas emission-based attribution includes both the effects as GHGs and the effects caused by stratospheric ozone depletion, specifically those estimated using equivalent effective stratospheric chlorine (EESC). Furthermore, forcing-based aerosols only involve the direct effects of sulfate, nitrate, primary organic aerosols (POA), secondary organic aerosols (SOA), black carbon (BC), and dust. However, emission-based aerosols cover not only the direct effects, but also the effects on tropospheric ozone and methane lifetime with regard to the OH sink, as well as the indirect effects from aerosol-cloud interaction (see Table S5 in ref (Su et al. 2022), SPM.5 in ref (IPCC 2013) for the relationship between emitted compounds/emissions and forcing agents).

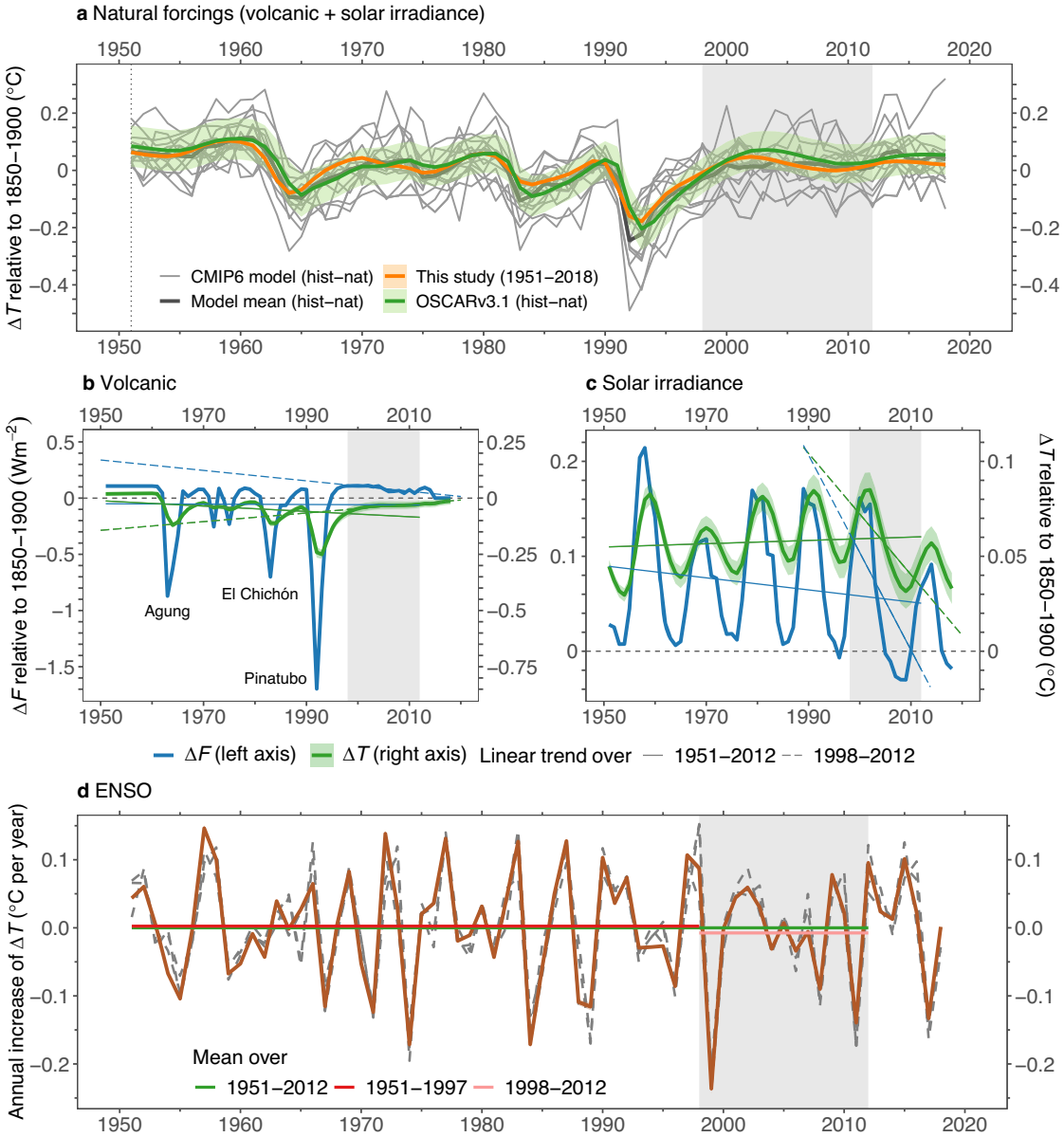

Fig. 4 | ΔT due to natural forces. a Natural forcing ΔT from OSCAR v3.1[52] and CMIP6 Earth System Models (ESMs)[53] (ensemble mean for each ESM, Supplementary Table 3), as well as this study. OSCAR v3.1 uncertainty denotes the one-sigma obtained from Monte Carlo simulations with n = 1000. **b** and **c** illustrate ΔF and ΔT for volcanic eruptions and solar irradiance, respectively. In **b** and **c**, thin solid and solid with extended dashed lines represent linear trends for the years 1951-2012 and 1998-2012, respectively. Three large volcanic eruptions are indicated in **b**. **d** Annual increase of ΔT caused by ENSO (see Supplementary Fig. 12 for the ENSO ΔT trend). Grey dashed lines in **d** depict annual increases of ΔT estimated using other ENSO indices shown in Supplementary Figs. 13-15. Thick horizontal lines represent the mean values for the specified periods. The ΔT ranges of this study in **a**-**d** are the one-sigma produced by the ensemble of statistical regressions. The warming slowdown era from 1998 to 2012 is shaded in light grey.

The conception of DDT gives a measurable indicator of the magnitude of change in the decadal trend. Using DDT, we captured both direct cooling contributions and slowing trends of ΔT in the warming slowdown. However, the DDT may be sensitive to the chosen reference period or endpoints, particularly if there is striking annual volatility. First, if a shorter reference period, such as 1970-2012, or a longer reference period, such as 1951-2018, was utilized, the amount of DDT for each factor may differ slightly. However, their contributions to the warming slowdown are robust (Supplementary Figs. 17–18). Second, the 15-year running trends (Fig. 5) implied that, for certain factors with considerable annual changes, such as volcanic activity, solar irradiance and ENSO, their annual signals are so powerful that they may control the trend of the warming slowdown. However, for relatively slow-response components such as methane and ODS, as well as other anthropogenic causes, trends are consistent and persistent. As a result, the warming slowdown is a combination of fast and slow responses driven by both anthropogenic and natural factors.

We utilized ENSO to depict internal variability, as it exerts a greater impact on global ΔT compared to other modes of variability[3,11,26,65]. The total sum of the DDT of individual factors converged on the observation (Fig. 2m), explaining almost all of the ΔT slowdown during the warming slowdown period. The use of different independent observations (Supplementary Figs. 19–21) or ENSO indices (Supplementary Figs. 22–24) gave similar results, implying that our analysis is quantitatively robust. On the other hand, we tested other modes of variability, such as the Atlantic Multidecadal Oscillation (AMO), the Pacific Decadal Oscillation (PDO), the North Atlantic Oscillation (NAO), and the Dipole Mode Index (DMI)

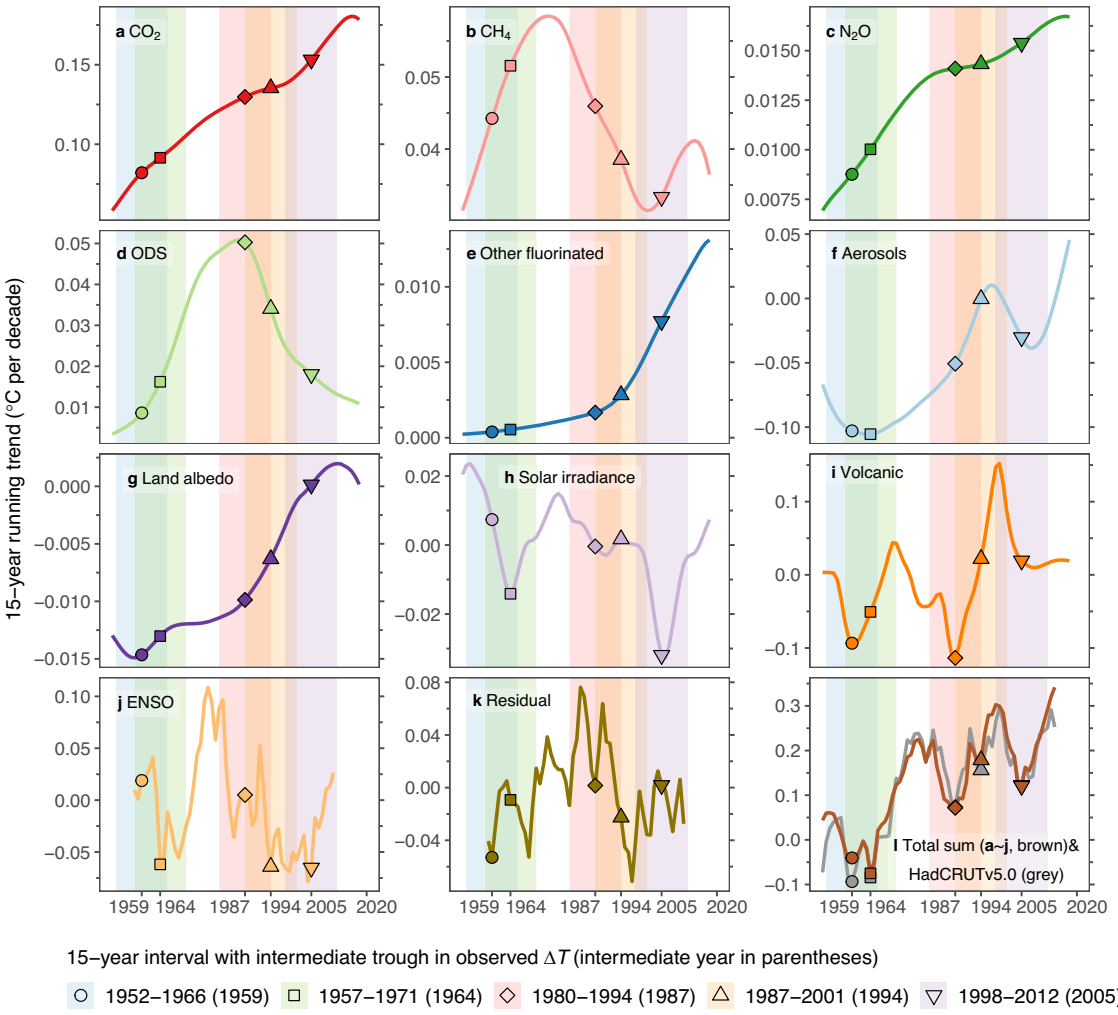

Fig. 5 | 15-year running trends for anthropogenic and natural ΔT. **a** to **j** represent individual anthropogenic and natural factors. **k** indicates the residual term of the statistical model. The total sum and HadCRUT5 are depicted in **l**. The vertical colour ribbons represent 15-year intervals with intermediate troughs (marked by colour points) in the observed global ΔT.

(Supplementary Figs. 25–28; see Data availability for the data sources). The other modes demonstrated inferior goodness-of-fit, with lower R-squared values in the regressions and a lower correlation between the estimated and observed values (Supplementary Tables 4–7). Furthermore, calculations using multiple modes such as MEI, AMO, PDO, and NAO, or two modes with prominent impacts like MEI and AMO, showed that different modes would alter the warming trend between 1998 and 2012 to varying degrees (Supplementary Figs. 29–30). The multiple- or two-mode regression produced a larger residual term, although the BIC was lower (Supplementary Table 1). The modes other than MEI implied smaller contributions to the DDT. Our analysis suggests that the ENSO index is a better indication of the primary annual perturbation in observed global ΔT.

Despite the presence of noticeable annual variations in the residuals, the overall deviation from the expected values (as indicated by the DDT of the residuals in Fig. 2) was minimal and would not impact our conclusion. The uncertainties may result from the autocorrelation of chosen predictors and cross-correlation among the predictors, as well as observational errors or inaccurate depictions of the real processes[3]. The correlation between simulated ΔT and observed ΔT here is higher than Lean's (2018) statistical method (r= 0.91 for space-based model during 1979-2017), most likely due to the full consideration of all available factors, which were derived from a physical RCM. This is also due to the use of the latest temperature record, while the older version may overmeasure the warming slowdown, resulting in larger residuals and lower goodness-of-fit (lower R-squared values) in the regression (Supplementary Fig. 31, Supplementary Tables 4-7). Therefore, our causal explanation of the warming slowdown is sound.

Combining a physical RCM and an observationally constrained statistical model, we comprehensively evaluated the relative contributions to the warming slowdown from 1998-2012. Our results show that carbon dioxide, aerosols and pollutants and erupting volcanoes principally accelerated global ΔT during the warming slowdown period compared to 1951-2012, whereas La Niña cooling and a descending solar cycle strongly offset the increased ΔT, accounting for approximately 50% and 26% of the total warming slowdown during 1998-2012 compared to 1951-2012. In particular, we identified that the reduced ODS and methane emissions also contributed approximately 13% and 11% of the total warming slowdown, which can be explained by the recorded atmospheric ΔC. Various factors superimposed on the timeline, slowing ΔT between 1998 and 2012, while the ENSO alone was insufficient to offset the warming trends caused by anthropogenic and natural forcings. The contribution of reduced ODS and methane was comparable in scale to La Niña cooling and the descending solar cycle, as well as the overall downward trend exhibited by the temperature records (Fig. 2m), all of which can be detected with instruments, either directly or indirectly. Thus, our findings provide practical evidence for preventing global warming by reducing GHG emissions.

Methods

ΔT simulations

We used an RCM - SCM4OPT v3.3[30–33] to simulate global ΔT trends resulting from anthropogenic factors (such as CO_2, CH_4, N_2O, halogenated gases (16 ODS and 23 other fluorinated gases), carbon monoxide (CO), nitrogen oxide (NO_x), volatile organic compounds (VOCs), sulfate (SO_x), black carbon (BC), organic carbon (OC), and land albedo) and natural forcings (such as volcanic and solar irradiance). SCM4OPT v3.3 was created by updating an older version, SCM4OPT v3.2[33]. We present a new parameterization for CH_4 forcing[66]. The methane ΔT trend in this study was estimated using a hybrid of the new Etminan parameterization and a traditional technique as in AR5[67], and the associated processes and parameters were used in the Monte Carlo simulation as below. The Etminan's method showed a 25% higher CH_4 forcing than the AR5's one (1750-2011), resulting in a lower DDT level of -0.015 ± 0.008 °C/decade (cf. -0.012 ± 0.007 °C/decade using AR5's estimation) in the final attribution (Supplementary Figs. 32–33).

A normalized marginal method[27,28,68,69] was applied to SCM4OPT v3.3 for ΔT quantifications of climate forcers. ΔT trends induced by nonemission factors such as natural forcings including volcanoes and solar irradiance, as well as human factors such as land albedo resulting from land-use change, were quantified using a residual method: (1) one historical emulation with all emissions and nonemission factors as input; (2) one "exclusive" experiment for estimating land-use albedo ΔT trends with constant preindustrial land cover levels, and two "exclusive" experiments for estimating natural forcing ΔT trends by deleting volcanic or solar forcings from historical emulations. We compared ΔT obtained from historical and "exclusive" experiments, and the differences between the two experiments were ΔT trends caused by these nonemission factors. For the remaining ΔT, the normalized marginal method was used to quantify the emission-induced ΔT trends[33]. We assumed that the ratio of a emission's (e) ΔT to overall ΔT, defined as α_e^t, is proportional to the marginal effect of e divided by the total marginal effect. To estimate α_e^t, two simulations were carried out for each species: (1) one historical simulation as above and the resulting ΔT denoted as ΔT_{all}; and (2) another identical simulation except emission e reduced by a fraction of ϵ = 0.001 to calculate the ΔT termed as $\Delta T_{e,\epsilon}$. Therefore, the relative contribution α_e^t can be obtained:

$$\alpha_e^t = \frac{\Delta T_{all} - \Delta T_{e,\epsilon}}{\sum_{e'} \left(\Delta T_{all} - \Delta T_{e',\epsilon}\right)} \quad (1)$$

ΔT_e resulting from emission e can be calculated as follows:

$$\Delta T_e = \Delta T_{all} \cdot \alpha_e^t \quad (2)$$

After calculating ΔT induced by emissions and nonemission factors, we classified the resulting ΔT as CO_2, CH_4, N_2O, ODS, other fluorinated gases, aerosols and pollutants, land albedo, volcanoes, and solar irradiance, considering their inherent characteristics and annual increases since the preindustrial revolution.

To estimate ΔT trends induced by GHGs ΔC (Fig. 3, Supplementary Fig. 10), we again used the above normalized marginal method for the forcing-driven mode of SCM4OPT v3.3. We calculated the associated ΔF from ΔC and applied ϵ = 0.001 to ΔF to obtain the trend of ΔC-induced ΔT. The same β_{GHG} (as below) was multiplied to estimate the final ΔT induced by the GHG ΔC.

It is worth noting that the numbers of ODS or other fluorinated gases used in this study differ from the compiled data or observations (Supplementary Table 2, Supplementary Fig. 9). For example, a few ODS gases (such as CFC-13, CH_2Cl_2 and $CHCl_3$) and other fluorinated gases (such as SO_2F_2, C_7F_{16}, C_8F_{18} and C_2Cl_4) were not included in our simulation due to data availability. However, the warming effects from these gases are relatively small, and our results retained almost the same total equivalent ΔC trends as the observations (Fig. 3, Supplementary Fig. 10). Therefore, our conclusions are unaffected.

Statistical model

ENSO has larger influences on the global ΔT than other internal variabilities[3,11,26,65]. We used ENSO to reflect the main changes due to internal variability. SCM4OPT v3.3 does not replicate ENSO. We employed a statistical model to correct the biases in the magnitude of the simulated ΔT, and distinguish ENSO influences from the observed ΔT[8,11,26]. We tested a set of statistical models with various predictors because the trends and magnitudes of the individual factors vary and can lead to overfitting of certain factors. The model with the lowest Bayesian information criterion (BIC) was selected to prevent overfitting (Supplementary Table 1). Therefore, we hypothesized that the observed ΔT consists of ΔT induced by categorized elements such as anthropogenic GHG emissions, other anthropogenic factors such as aerosols and pollutants and land albedo, natural forcings, and ENSO. Accordingly, the observed ΔT is defined as a multiple regression among the time series of these elements plus a residual component allowing for errors resulting from simulations and observations:

$$\begin{aligned}\Delta T_{obs}(t) = {} & \beta_{GHG}(\Delta T_{CO_2}(t) + \Delta T_{CH_4}(t) + \Delta T_{N_2O}(t) + \Delta T_{ODS}(t) \\ & + \Delta T_{oFGS}(t)) + \beta_{non-GHG}(\Delta T_{aero}(t) + \Delta T_{lcc}(t)) \\ & + \beta_{nat}(\Delta T_{volc}(t) + \Delta T_{solar}(t)) + \beta^1_{MEI} MEI(t-\tau_1) \\ & + \beta^2_{MEI} MEI(t-\tau_2) + \beta^3_{MEI} MEI(t-\tau_3) + Resi(t) + T_0\end{aligned} \quad (3)$$

where $\Delta T_{obs}(t)$ is the observed ΔT. $\Delta T_{CO_2}(t)$, $\Delta T_{CH_4}(t)$, $\Delta T_{N_2O}(t)$, $\Delta T_{ODS}(t)$, $\Delta T_{oFGS}(t)$, $\Delta T_{aero}(t)$, $\Delta T_{lcc}(t)$, $\Delta T_{volc}(t)$ and $\Delta T_{solar}(t)$ indicate the simulated ΔT caused by CO_2, CH_4, N_2O, ODS, other fluorinated gases, aerosols and pollutants, land albedo, volcanoes and solar irradiance, respectively. β_{GHG}, $\beta_{non-GHG}$ and β_{nat} are fitted coefficients for the associated factors. $MEI(t)$ indicates the monthly multivariate ENSO index (MEI) taken from existing literature[70]. Before applying the MEI, we eliminated the linear trend from it. β^i_{MEI} and τ_i (i = 1, 2, 3) represent the fitted coefficients and the delayed months for the MEI, respectively, which were selected to maximize the variance explained (Supplementary Tables 4-7). $Resi(t)$ and T_0 are the residuals and intercept, respectively. The time series of the ΔT values estimated from SCM4OPT v3.3 are bimonthly data, which we linearly interpolated into monthly values before employing in the statistical model. We applied multiple regression to the data from 1951 to 2018. The fitted coefficients, R^2 values and correlation coefficients are shown in Supplementary Tables 4-7.

Uncertainties

This study considered uncertainties in historical emissions, climate model uncertainties, and uncertainties found in various observation records. First, four emission datasets, i.e., the Community Emissions Data System (CEDS)[48], Emission Database for Global Atmospheric Research (EDGAR) v7.0_GHG 1970-2021 and EDGAR v6.1_AP 1970-2018[71,72], ACCMIP[73], and BB4CMIP[74] were used to represent uncertainties resulting from estimates of historical emissions. Hence, our results reflect the warming caused by the release of GHG emissions, as well as aerosols and pollutants from various sectors such as agriculture, commercial and residential, energy, industrial, transport, and waste management. Furthermore, the temperature changes resulting from aerosols and pollutants emitted by agricultural waste burning, residential biomass burning, or large-scale forest and grass fires are also incorporated based on the data available in these datasets. We compiled and processed the data in the same way as in Su et al.[33]. When a certain species was not available, we used equivalent emission data from a separate dataset. These emissions were used to generate the atmospheric ΔC and the associated ΔF, and then to estimate the global ΔT. Second, we performed a Monte Carlo simulation with n = 1000 (see Table S4 in the forcing study[33] for the parameter sets) for the climate system to calculate the climate model uncertainties. Third, we carried out regressions for individual temperature records or the representative record HadCRUT5 with different ENSO indices, considering that ENSO effects and residuals are somewhat sensitive to the temperature records and ENSO indices.

The statistical regression was also performed using the Monte Carlo method with n = 1000. For example, the observed value was randomly chosen from the available dataset ensemble (for HadCRUT5 n = 200), while the predictor variables were randomly selected from the ensemble of SCM4OPTv3.3 simulations.

To estimate the uncertainty of aerosols presented in Supplementary Fig. 2, we summed the aerosols' ΔT from AR6, namely, NO_x, VOC, SO_2, OC, BC and NH_3. Their uncertainties were propagated by assuming that the individual ΔT values are independent variables that are normally distributed. Thus, their sum was also normally distributed. For example, from $X \sim N(\mu_X, \sigma_X^2)$ and $Y \sim N(\mu_Y, \sigma_Y^2)$, we obtained the uncertainty of $Z = X + Y$: $Z \sim N(\mu_X + \mu_Y, \sigma_X^2 + \sigma_Y^2)$. A similar estimation was used in the AR6 calculation (https://github.com/sarambl/AR6_CH6_RCMIPFIGS).

Data availability

The data used in this analysis can be accessed online (last access for all, 22 May 2023): Coupled Model Intercomparison Project 6 (CMIP6) (https://esgf-node.llnl.gov/projects/cmip6/); Community Emissions Data System (CEDS) (https://esgf-node.llnl.gov/search/input4mips/); Emission Database for Global Atmospheric Research (EDGAR) v7.0 (Global Greenhouse Gas Emissions) (https://edgar.jrc.ec.europa.eu/dataset_ghg70); EDGAR v6.1 (Global Air Pollutant Emissions) (https://edgar.jrc.ec.europa.eu/dataset_ap61); Coupled Model Intercomparison Project Phase 6 (CMIP6) emissions from the Integrated Assessment Modeling Consortium (IAMC) (https://esgf-node.llnl.gov/search/input4mips/); The Atmospheric Chemistry and Climate Model Intercomparison Project (ACCMIP)[73] (https://tntcat.iiasa.ac.at/RcpDb); Carbon emissions from land use and land-cover change[75,76] (http://www.globalcarbonatlas.org/en/CO2-emissions); Land-use change emissions from ref. 77 (https://cdiac.ess-dive.lbl.gov/ftp/Smith_Rothwell_Land-Use_Change_Emissions/); Land-Use Harmonization (LUH2) (https://luh.umd.edu/); Historical greenhouse gas concentrations for climate modelling (CMIP6) (https://doi.org/10.5194/gmd-10-2057-2017); National Oceanic & Atmospheric Administration Carbon Cycle Greenhouse Gases (atmospheric concentrations of CO_2, CH_4 and N_2O) (https://gml.noaa.gov/ccgg/); The NOAA Ozone Depleting Gas Index (https://gml.noaa.gov/odgi/); Advanced Global Atmospheric Gases Experiment (AGAGE) (https://agage.mit.edu/data/agage-data); The Global Carbon Project (GCP)[78] (https://www.globalcarbonproject.org); Global Methane Budget (https://www.globalcarbonproject.org/methanebudget/); Hadley Centre/Climatic Research Unit Temperature (HadCRUT) v5.0 (https://www.metoffice.gov.uk/hadobs/hadcrut5/); Berkeley Earth (Global Temperature Data) (https://berkeleyearth.org/data/); NOAAGlobalTemp v5.1 (https://www.ncei.noaa.gov/products/land-based-station/noaa-global-temp); GISS Surface Temperature Analysis (GISTEMP v4) (https://data.giss.nasa.gov/gistemp/); NOAA MEI[70] (https://psl.noaa.gov/enso/mei.old/mei.html); MEI from NCEP-NCAR (https://www.webberweather.com/multivariate-enso-index.html); Cold Tongue Index (CTI) (https://github.com/ToddMitchellGH/Cold-Tongue-Index); "BEST" ENSO Index[79] (https://psl.noaa.gov/people/cathy.smith/best/). Atlantic Multidecadal Oscillation (AMO) (https://www1.ncdc.noaa.gov/pub/data/cmb/ersst/v5/index/ersst.v5.amo.dat). Pacific Decadal Oscillation (PDO) (https://www.ncei.noaa.gov/pub/data/cmb/ersst/v5/index/ersst.v5.pdo.dat). North Atlantic Oscillation (NAO) (https://psl.noaa.gov/gcos_wgsp/Timeseries/Data/nao.long.data). Dipole Mode Index (DMI) (https://psl.noaa.gov/gcos_wgsp/Timeseries/Data/dmi.had.long.data). The detailed results are available to download from (10.5281/zenodo.12514221).

Code availability

All code used in this study is available from the corresponding author upon reasonable request.

Received: 11 October 2023; Accepted: 24 September 2024;
Published online: 01 November 2024

References

1. Stocker, T. et al. *Technical Summary*, book section TS, 33–115 (Cambridge University Press, Cambridge, United Kingdom and New York, NY, USA, 2013).
2. Simmons, A. J. et al. A reassessment of temperature variations and trends from global reanalyses and monthly surface climatological datasets. *Q. J. R. Meteorological Soc.* **143**, 101–119 (2017).
3. Lean, J. L. Observation-based detection and attribution of 21st century climate change. *WIREs Clim. Change* **9**, e511 (2018).
4. Eyring, V. et al. *Human influence on the climate system*, book section 3 (Cambridge University Press, Cambridge, United Kingdom and New York, NY, USA, 2021).
5. Kosaka, Y. & Xie, S. P. Recent global-warming hiatus tied to equatorial Pacific surface cooling. *Nature* **501**, 403–407 (2013).
6. Watanabe, M. et al. Contribution of natural decadal variability to global warming acceleration and hiatus. *Nat. Clim. Change* **4**, 893–897 (2014).
7. Brown, P. T., Li, W. & Xie, S.-P. Regions of significant influence on unforced global mean surface air temperature variability in climate models. *J. Geophys. Res.: Atmosph.* **120**, 480–494 (2015).
8. Dai, A., Fyfe, J. C., Xie, S.-P. & Dai, X. Decadal modulation of global surface temperature by internal climate variability. *Nat. Clim. Change* **5**, 555–559 (2015).
9. Steinman, B. A., Mann, M. E. & Miller, S. K. Atlantic and Pacific multidecadal oscillations and Northern Hemisphere temperatures. *Science* **347**, 988–991 (2015).
10. Pasini, A., Triacca, U. & Attanasio, A. Evidence for the role of the Atlantic multidecadal oscillation and the ocean heat uptake in hiatus prediction. *Theor. Appl. Climatol.* **129**, 873–880 (2017).
11. Lean, J. L. & Rind, D. H. How natural and anthropogenic influences alter global and regional surface temperatures: 1889 to 2006. *Geophys. Res. Lett.* **35** (2008).
12. Solomon, S. et al. The Persistently Variable "Background" Stratospheric Aerosol Layer and Global Climate Change. *Science* **333**, 866–870 (2011).
13. Haywood, J. M., Jones, A. & Jones, G. S. The impact of volcanic eruptions in the period 2000–2013 on global mean temperature trends evaluated in the HadGEM2-ES climate model. *Atmos. Sci. Lett.* **15**, 92–96 (2014).
14. Ridley, D. A. et al. Total volcanic stratospheric aerosol optical depths and implications for global climate change. *Geophys. Res. Lett.* **41**, 7763–7769 (2014).
15. Huber, M. & Knutti, R. Natural variability, radiative forcing and climate response in the recent hiatus reconciled. *Nat. Geosci.* **7**, 651–656 (2014).
16. Santer, B. D. et al. Volcanic contribution to decadal changes in tropospheric temperature. *Nat. Geosci.* **7**, 185–189 (2014).
17. Deser, C., Guo, R. & Lehner, F. The relative contributions of tropical Pacific sea surface temperatures and atmospheric internal variability to the recent global warming hiatus. *Geophys. Res. Lett.* **44**, 7945–7954 (2017).
18. Wang, C.-Y., Xie, S.-P., Kosaka, Y., Liu, Q. & Zheng, X.-T. Global influence of tropical pacific variability with implications for global warming slowdown. *J. Clim.* **30**, 2679 – 2695 (2017).
19. Estrada, F., Perron, P. & Martínez-López, B. Statistically derived contributions of diverse human influences to twentieth-century temperature changes. *Nat. Geosci.* **6**, 1050–1055 (2013).
20. Lu, Q.-B. Major Contribution of Halogenated Greenhouse Gases to Global Surface Temperature Change. *Atmosphere.* **13** (2022).
21. Solomon, S. et al. Contributions of Stratospheric Water Vapor to Decadal Changes in the Rate of Global Warming. *Science* **327**, 1219–1223 (2010).
22. Schmidt, G. A., Shindell, D. T. & Tsigaridis, K. Reconciling warming trends. *Nat. Geosci.* **7**, 158–160 (2014).

23. Medhaug, I., Stolpe, M. B., Fischer, E. M. & Knutti, R. Reconciling controversies about the 'global warming hiatus'. *Nature* **545**, 41–47 (2017).
24. Hedemann, C., Mauritsen, T., Jungclaus, J. & Marotzke, J. The subtle origins of surface-warming hiatuses. *Nat. Clim. Change* **7**, 336–339 (2017).
25. Power, S., Delage, F., Wang, G., Smith, I. & Kociuba, G. Apparent limitations in the ability of CMIP5 climate models to simulate recent multi-decadal change in surface temperature: implications for global temperature projections. *Clim. Dyn.* **49**, 53–69 (2017).
26. Foster, G. & Rahmstorf, S. Global temperature evolution 1979–2010. *Environ. Res. Lett.* **6**, 044022 (2011).
27. Trudinger, C. & Enting, I. Comparison of formalisms for attributing responsibility for climate change: Non-linearities in the Brazilian Proposal approach. *Clim. Chan.* **68**, 67–99 (2005).
28. Li, B. et al. The contribution of China's emissions to global climate forcing. *Nature* **531**, 357–361 (2016).
29. Fu, B. et al. Short-lived climate forcers have long-term climate impacts via the carbon–climate feedback. *Nat. Clim. Change* **10**, 851–855 (2020).
30. Su, X. et al. Emission pathways to achieve 2.0°C and 1.5°C climate targets. *Earth's. Future* **5**, 592–604 (2017).
31. Su, X. et al. How do climate-related uncertainties influence 2 and 1.5 °C pathways? *Sustain. Sci.* **13**, 291–299 (2018).
32. Nicholls, Z. et al. Reduced Complexity Model Intercomparison Project Phase 2: Synthesizing Earth System Knowledge for Probabilistic Climate Projections. *Earth's. Future* **9**, 1–25 (2021).
33. Su, X., Tachiiri, K., Tanaka, K., Watanabe, M. & Kawamiya, M. Identifying crucial emission sources under low forcing scenarios by a comprehensive attribution analysis. *One Earth* **5**, 1–13 (2022).
34. IPCC. Summary for policymakers. In Masson-Delmotte, V. et al. (eds.) *Climate Change 2021: The Physical Science Basis. Contribution of Working Group I to the Sixth Assessment Report of the Intergovernmental Panel on Climate Change*, book section SPM (Cambridge University Press, Cambridge, UK and New York, NY, USA, 2021).
35. Cionni, I. et al. Ozone database in support of cmip5 simulations: results and corresponding radiative forcing. *Atmos. Chem. Phys.* **11**, 11267–11292 (2011).
36. Conley, A. J., Lamarque, J.-F., Vitt, F., Collins, W. D. & Kiehl, J. Port, a cesm tool for the diagnosis of radiative forcing. *Geosci. Model Dev.* **6**, 469–476 (2013).
37. Checa-Garcia, R., Hegglin, M. I., Kinnison, D., Plummer, D. A. & Shine, K. P. Historical Tropospheric and Stratospheric Ozone Radiative Forcing Using the CMIP6 Database. *Geophys. Res. Lett.* **45**, 3264–3273 (2018).
38. Skeie, R. B. et al. Historical total ozone radiative forcing derived from CMIP6 simulations. *npj Clim. Atmosph. Sci.* **3** (2020).
39. Chiodo, G. & Polvani, L. M. New Insights on the Radiative Impacts of Ozone-Depleting Substances. *Geophys. Res. Lett.* **49**, 1–11 (2022).
40. Ramaswamy, V., Schwarzkopf, M. D. & Shine, K. P. Radiative forcing of climate from halocarbon-induced global stratospheric ozone loss. *Nature* **355**, 810–812 (1992).
41. Shindell, D. et al. Attribution of historical ozone forcing to anthropogenic emissions. *Nat. Clim. Change* **3**, 567–570 (2013).
42. Nisbet, E. G., Dlugokencky, E. J. & Bousquet, P. Methane on the Rise-Again. *Science* **343**, 493–495 (2014).
43. Nisbet, E. G. et al. Rising atmospheric methane: 2007–2014 growth and isotopic shift. *Glob. Biogeochem. Cycles* **30**, 1356–1370 (2016).
44. Rigby, M. et al. Renewed growth of atmospheric methane. *Geophys. Res. Lett.* **35**, 2–7 (2008).
45. Dlugokencky, E. J. et al. Observational constraints on recent increases in the atmospheric CH_4 burden. *Geophys. Res. Lett.* **36**, 3–7 (2009).
46. Montzka, S. A., Dlugokencky, E. J. & Butler, J. H. Non-CO_2 greenhouse gases and climate change. *Nature* **476**, 43–50 (2011).
47. Meinshausen, M. et al. Historical greenhouse gas concentrations for climate modelling (CMIP6). *Geosci. Model Dev.* **10**, 2057–2116 (2017).
48. Hoesly, R. M. et al. Historical (1750–2014) anthropogenic emissions of reactive gases and aerosols from the Community Emissions Data System (CEDS). *Geosci. Model Dev.* **11**, 369–408 (2018).
49. CHANDRA, N. et al. Emissions from the Oil and Gas Sectors, Coal Mining and Ruminant Farming Drive Methane Growth over the Past Three Decades. *J. Meteorol. Soc. Jpn. Ser. II* **99**, 309–337 (2021).
50. Montzka, S. et al. *Chapter 1: Ozone-Depleting Substances (ODSs) and Related Chemicals*, 1–108 (World Meteorological Organization, 2011).
51. Forster, P. et al. Changes in Atmospheric Constituents and in Radiative Forcing. In Solomon, S.et al. (eds.) *Climate Change 2007: The Physical Science Basis. Contribution of Working Group I to the Fourth Assessment Report of the Intergovernmental Panel on Climate Change*, book section 2 (Cambridge University Press, Cambridge, United Kingdom and New York, NY, USA, 2007).
52. Gasser, T. et al. Historical CO_2 emissions from land use and land cover change and their uncertainty. *Biogeosciences* **17**, 4075–4101 (2020).
53. Gillett, N. P. et al. The Detection and Attribution Model Intercomparison Project (DAMIP v1.0) contribution to CMIP6. *Geosci. Model Dev.* **9**, 3685–3697 (2016).
54. Wigley, T. M. L., Ammann, C. M., Santer, B. D. & Raper, S. C. B. Effect of climate sensitivity on the response to volcanic forcing. *J. Geophys. Res. Atmosph.* **110** (2005).
55. Gregory, J. M., Andrews, T., Good, P., Mauritsen, T. & Forster, P. M. Small global-mean cooling due to volcanic radiative forcing. *Clim. Dyn.* **47**, 3979–3991 (2016).
56. Takahashi, C. & Watanabe, M. Pacific trade winds accelerated by aerosol forcing over the past two decades. *Nat. Clim. Change* **6**, 768–772 (2016).
57. Geng, T. et al. Increased occurrences of consecutive La Niña events under global warming. *Nature* **619**, 774–781 (2023).
58. Cai, W. et al. Anthropogenic impacts on twentieth-century ENSO variability changes. *Nat. Rev. Earth Environ.* **4**, 407–418 (2023).
59. Hansen, J. et al. Climate impact of increasing atmospheric carbon dioxide. *Science* **213**, 957–966 (1981).
60. Paudel, R., Mahowald, N. M., Hess, P. G. M., Meng, L. & Riley, W. J. Attribution of changes in global wetland methane emissions from pre-industrial to present using clm4.5-bgc. *Environ. Res. Lett.* **11**, 034020 (2016).
61. Reay, D. S., Smith, P., Christensen, T. R., James, R. H. & Clark, H. Methane and Global Environmental Change. *Annu. Rev. Environ. Resour.* **43**, 165–192 (2018).
62. Skeie, R. B., Hodnebrog, Ø. & Myhre, G. Trends in atmospheric methane concentrations since 1990 were driven and modified by anthropogenic emissions. *Commun. Earth Environ.* **4**, 317 (2023).
63. Saunois, M. et al. The Global Methane Budget 2000–2017. *Earth Syst. Sci. Data* **12**, 1561–1623 (2020).
64. Lauvaux, T. et al. Global assessment of oil and gas methane ultra-emitters. *Science* **375**, 557–561 (2022).
65. Thompson, D. W. J., Wallace, J. M., Jones, P. D. & Kennedy, J. J. Identifying signatures of natural climate variability in time series of global-mean surface temperature: Methodology and insights. *J. Clim.* **22**, 6120 – 6141 (2009).
66. Etminan, M., Myhre, G., Highwood, E. J. & Shine, K. P. Radiative forcing of carbon dioxide, methane, and nitrous oxide: A significant revision of the methane radiative forcing. *Geophys. Res. Lett.* **43**, 12,614–12,623 (2016).
67. Myhre, G. et al. *Anthropogenic and Natural Radiative Forcing*, book section 8, 659-740 (Cambridge University Press, Cambridge, United Kingdom and New York, NY, USA, 2013).

68. Fu, B. et al. The contributions of individual countries and regions to the global radiative forcing. *Proc. Natl. Acad. Sci.* **118** (2021).
69. Boucher, O., Borella, A., Gasser, T. & Hauglustaine, D. On the contribution of global aviation to the CO_2 radiative forcing of climate. *Atmos. Environ.* **267**, 118762 (2021).
70. Wolter, K. & Timlin, M. S. El Niño and Southern Oscillation behaviour since 1871 as diagnosed in an extended multivariate ENSO index (MEI.ext). *Int. J. Climatol.* **31**, 1074–1087 (2011).
71. Crippa, M. et al. GHG emissions of all world: 2021 report. Tech. Rep. (2021).
72. Crippa, M. et al. CO_2 emissions of all world countries – JRC/IEA/PBL 2022 Report. Tech. Rep. (2022).
73. Lamarque, J.-F. et al. The Atmospheric Chemistry and Climate Model Intercomparison Project (ACCMIP): overview and description of models, simulations and climate diagnostics. *Geosci. Model Dev.* **6**, 179–206 (2013).
74. van Marle, M. J. E. et al. Historic global biomass burning emissions for CMIP6 (BB4CMIP) based on merging satellite observations with proxies and fire models (1750–2015). *Geosci. Model Dev.* **10**, 3329–3357 (2017).
75. Houghton, R. A. et al. Carbon emissions from land use and land-cover change. *Biogeosciences* **9**, 5125–5142 (2012).
76. Hansis, E., Davis, S. J. & Pongratz, J. Relevance of methodological choices for accounting of land use change carbon fluxes. *Glob. Biogeochem. Cycles* **29**, 1230–1246 (2015).
77. Smith, S. J. & Rothwell, A. Carbon density and anthropogenic land-use influences on net land-use change emissions. *Biogeosciences* **10**, 6323–6337 (2013).
78. Friedlingstein, P. et al. Global Carbon Budget 2020. *Earth Syst. Sci. Data* **12**, 3269–3340 (2020).
79. Smith, C. A. & Sardeshmukh, P. D. The effect of ENSO on the intraseasonal variance of surface temperatures in winter. *Int. J. Climatol.* **20**, 1543–1557 (2000).

Acknowledgements

This work was supported by the Decarbonized and Sustainable Society Research Program at the National Institute for Environmental Studies, Japan, and the Program for the advanced studies of climate change projection (SENTAN, Grant Number JPMXD0722681344) from the Ministry of Education, Culture, Sports, Science and Technology (MEXT), Japan. K. Tanaka benefited from state assistance managed by the National Research Agency in France under the Programme d'Investissements d'Avenir under the reference ANR-19-MPGA-0008. The computational resources were provided by the National Institute for Environmental Studies (NIES), Japan, and Japan Agency for Marine-Earth Science and Technology (JAMSTEC).

Author contributions

X.S. designed the study, performed the simulations, produced all figures. H.S. provided insights to create the statistical model. X.S. led the writing with contributions from H.S., K.Tanaka, K.Tachiiri, T.H., M.W., M.K., K.Takahashi and T.Y.

Competing interests

The authors declare no competing interests.

Additional information

Supplementary information The online version contains supplementary material available at https://doi.org/10.1038/s43247-024-01723-x.

Correspondence and requests for materials should be addressed to Xuanming Su.

Peer review information *Communications Earth & Environment* thanks the anonymous reviewers for their contribution to the peer review of this work. Primary Handling Editors: Kyung-Sook Yun, Heike Langenberg, Alienor Lavergne. A peer review file is available.